Amine-Functionalized Silane-Assisted Preparation of AgNP-Deposited α-Ni(OH)$_2$ Composite Materials and Their Application in Hg^{2+} Ion Sensing

Manickam Sundarapandi, Raju Praveen, Sivakumar Shanmugam,* and Ramasamy Ramaraj*

Read Online

ACCESS | Metrics & More | Article Recommendations | SI Supporting Information

ABSTRACT: A facile synthetic methodology for the deposition of different concentrations of Ag nanoparticles (AgNPs) on α-Ni(OH)$_2$ sheets (α-Ni$_1$(OH)$_2$-Ag$_{0.5}$, α-Ni$_1$(OH)$_2$-Ag$_1$, α-Ni$_1$(OH)$_2$-Ag$_2$, and α-Ni$_1$(OH)$_2$-Ag$_3$) is reported using N-[3-(trimethoxysilyl)propyl]-diethylenetriamine (TPDT) silane. The TPDT aminosilane facilitates the formation of α-Ni(OH)$_2$ sheets and reduces the Ag$^+$ precursor to AgNPs, leading to the deposition of AgNPs on α-Ni(OH)$_2$ sheets. UV−vis absorption spectroscopy, transmission microscopy analyses, X-ray photoelectron spectroscopy, X-ray diffraction, and attenuated total reflectance−Fourier transform infrared spectroscopy techniques were used to characterize the prepared α-Ni$_1$(OH)$_2$-Ag$_{0.5-3}$ composite materials. High-angle annular dark-field scanning transmission electron microscopy−energy-dispersive X-ray spectroscopy mapping images and scanning electron microscopy−energy-dispersive X-ray spectroscopy mapping images were recorded to understand the α-Ni$_1$(OH)$_2$-Ag composite sheet materials. The optical sensing property of α-Ni$_1$(OH)$_2$-Ag$_{0.5-3}$ composite materials toward toxic Hg^{2+} ions were investigated using a UV−vis absorption spectroscopy technique. The α-Ni$_1$(OH)$_2$-Ag$_2$ composite material showed selective sensing behavior.
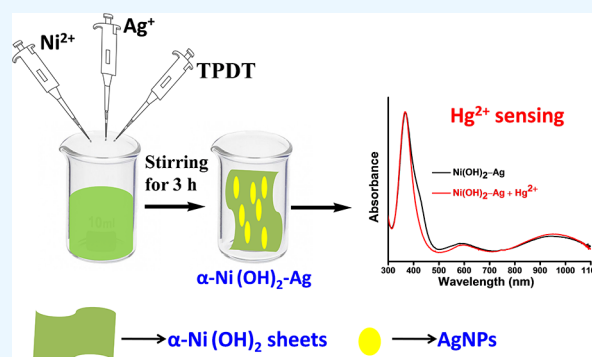
1. INTRODUCTION

The shape control of inorganic nanomaterials has attracted attention due to their unique functions in electrical, magnetic, optical, and catalytic properties.[1−4] Especially, Ni-containing nanomaterials have received significant attention among 3d transition metal series because of their earth-abundant nature.[5] Among various forms of Ni-containing nanomaterials, such as NiO, Ni(OH)$_2$, NiOOH, NiS, and NiSe have attracted more attention due to their applications in various fields, such as batteries, fuel cells, catalysis, and sensors.[6,7] Inspired by the potential use of Ni(OH)$_2$, the synthesis of Ni(OH)$_2$ with various morphologies such as flower-like forms,[8] nanobelts,[9] nanorods[10] and microspheres[11] have been reported. Ni(OH)$_2$ shows hexagonal layered structures with two polymorphs, i.e., α-Ni(OH)$_2$ and β-Ni(OH)$_2$, with two different interlayer spaces (α: 7 Å and β: ~4.6 Å) and their arrangements.[8] α-Ni(OH)$_2$ nanoparticles (NPs) shows good electrochemical properties than that of β-Ni(OH)$_2$ NPs,[8] and hence, the synthesis of α-Ni(OH)$_2$ NPs is of utmost concern. The optical and catalytic properties of pristine α-Ni(OH)$_2$ and modified α-Ni(OH)$_2$ have been reported.[12−15] However, a systematic investigation on the sensing behavior of the combination of α-Ni(OH)$_2$ and noble metal nanocatalysts using N-[3-(trimethoxysilyl)propyl]-diethylenetriamine (TPDT) silane was not reported. Especially, silver NP(AgNP)-based noble

metal nanocatalysts show potential applications relative to surface Plasmon resonance (SPR), chemical/biological sensors, and surface-enhanced Raman spectroscopy and are employed in antibacterial and antiviral medicines.[16−20] Generally, the colloidal phase synthesis of NPs are more advantageous since specified instruments are not needed and processing and assembling can easily be enforced.[21]

The recognition and sensing of mercury (Hg^{2+} ions) are of significant current interest since a very small quantity of Hg^{2+}ions can lead to severe damage to the central nervous and endocrine systems.[22] The recommended contaminant level of Hg^{2+} ions in food and drinking water is 0.002 mg L^{-1} (0.01 M) by the United States Environmental Protection Agency (EPA). Hence, designing new methods for the sensitive and selective detection of Hg^{2+} ions by a simple optical detection method will find application in both human health and environment aspects. Compared to conventional spectroscopic detection of Hg^{2+} ions, the colorimetric method is a simple method due to

their simplicity (naked eye detection), low cost, and fast detection.[21] The detection of Hg^{2+} ions using different nanomaterials with size-, shape-, and interparticle distance-dependent optical properties and high extinction coefficients have been reported.[23−27] Hence, the preparation of metal NPs with different morphologies by a facile method for selective sensing of Hg^{2+} ions is necessity.

In the present work, a facile preparation method at room temperature for depositing Ag_xNPs ($x = 0.5, 1, 2$ and 3) on α-$Ni_1(OH)_2$sheets (α-$Ni_1(OH)_2$-$Ag_{0.5−3}$) in the presence of TPDT silane without using any external reducing agent is reported. Upon varying the concentration of Ag^+ ions, the size of AgNPs also changed with the uniform deposition of AgNPs on the α-$Ni_1(OH)_2$ sheets. In the earlier reported methods, the α-$Ni_1(OH)_2$ sheets were prepared at higher temperature using a reducing agent and a stabilizing agent.[5,6] Here, the TPDT aminosilane is known to act as both reducing agent and stabilizing agent.[28] The sensing property of the prepared α-$Ni(OH)_2$-$Ag_{0.5−3}$ composite materials (CMs) toward the colorimetric sensing of toxic Hg^{2+} ions (Scheme 1) was

Scheme 1. Scheme Illustrating the Synthesis of α-$Ni(OH)_2$-Ag Composite Materials toward Hg^{2+} Ion Sensing
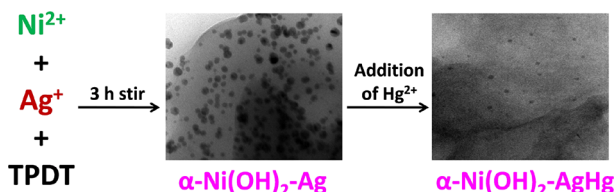
demonstrated based on the change in the SPR of AgNPs in the α-$Ni_1(OH)_2$-$Ag_{0.5−3}$CMs. Results revealed that the α-$Ni_1(OH)_2$-Ag_2 CM showed the selective sensing of Hg^{2+} ions than that of other CMs, pristine α-$Ni(OH)_2$/TPDT, and pristine AgNPs/TPDT.

2. EXPERIMENTAL SECTION

2.1. Materials. Nickel(II) chloride hexahydrate ($NiCl_2 \cdot 6H_2O$) and all other chemicals were purchased from Merck. *N*-[3(Trimethoxysilyl)propyl]diethylenetriamine (TPDT) and mercury(II) chloride were purchased from Sigma-Aldrich. All chemicals were used as received, and double-distilled water was used to prepare all the solutions.

2.2. Synthesis of the α-$Ni_1(OH)_2$-$Ag_{0.5−3}$ CMs. In the synthesis, 238 mg of $NiCl_2 \cdot 6H_2O$ was dissolved in 10 mL of double-distilled water in a round-bottom (RB) flask. The final concentration of Ni^{2+} was calculated from the above solution and taken as α-$Ni_1(OH)_2$ for convenience. To this RB flask, 20.25 μL of 10 mM Ag^+ was added and stirred for 10 min. To this solution, 0.5 mL of 50 mM TPDT silane was added and then stirred for 3 h to form AgNPs deposited on α-$Ni_1(OH)_2$ sheets (α-$Ni_1(OH)_2$-$Ag_{0.5}$ CM). Using the same protocol, α-$Ni_1(OH)_2$-Ag_1, α-$Ni_1(OH)_2$-Ag_2, and α-$Ni_1(OH)_2$-Ag_3 CMs with different concentrations were prepared. The subscript numbers indicate the molar ratio between Ni^{2+} and Ag. For comparison, bare α-$Ni_1(OH)_2$/TPDT and AgNPs/TPDT were prepared.

2.3. Optical and Colorimetric Sensing of Hg^{2+} Ions. Both optical and colorimetric sensing of Hg^{2+} ions were studied using spectrophotometric technique. For optical sensing, 5 μL of an aqueous solution of Hg^{2+} ions were

added to 2 mL of α-$Ni_1(OH)_2$-$Ag_{0.5−3}$ or pristine α-$Ni_1(OH)_2$/TPDT or AgNPs/TPDT solution and shaken well. After that, the absorption spectra were recorded after 2 min of addition, and the absorbance changes were monitored. For colorimetric sensing, an optimal concentration of Hg^{2+} ions and other possible interfering metal ions were added to 2 mL of α-$Ni_1(OH)_2$-Ag_2 CMs and shaken well, and the color changes were noted with naked eye.

2.4. Characterization. UV−vis absorption spectra were recorded using an Agilent Technologies 8453 spectrophotometer using a 1 cm quartz cell. Transmission electron microscopy (TEM) images were obtained with an FEI Tecnai G^2 20 S-TWIN instrument operated at 200 kV. High-angle annular dark-field scanning transmission electron microscopy−energy-dispersive X-ray spectroscopy (HAADF-STEM-EDS) images were obtained from an FEI Tecnai F20. Scanning electron microscopy−energy dispersive X−ray spectroscopy (SEM-EDS) mapping images were obtained on TESCAN VEGA3 SBH. X-ray photoelectron spectra (XPS) were recorded from a PHI 5000 Versa Probe III scanning microprobe with an Al K_α radiation source (1486.6 eV). X-ray diffraction (XRD) patterns were recorded with a XPERT-PRO diffractometer (λ = 1.54060 Å). Fourier transform infrared (FT-IR) spectra analyses were recorded using a Spectrum GX (PerkinElmer).

3. RESULTS AND DISCUSSION

3.1. Characterizations of the α-$Ni_1(OH)_2$-$Ag_{0.5−3}$ CMs. Sheet-like nickel hydroxide-silver (α-$Ni_1(OH)_2$-$Ag_{0.5−3}$) CMs were synthesized by a facile method at room temperature in the presence of *N*-[3(trimethoxysilyl)propyl]-diethylenetriamine (TPDT) silane without using any external reducing agent. The simultaneous formation of $Ni(OH)_2$ and reduction of Ag^+ ions to AgNPs led to the formation of α-$Ni_1(OH)_2$-Ag CMs. The TPDT aminosilane acts both as a reducing agent and as stabilizing agent. The α-$Ni_1(OH)_2$-$Ag_{0.5−3}$ CMs were successfully synthesized, and the formation was initially confirmed by recording the absorption spectra. The absorption spectrum of the pristine α-$Ni_1(OH)_2$ sheet colloidal solution showed the characteristic absorption bands at 364, 588, and 950 nm (Figure 1a).[12] The absorption bands observed for α-$Ni_1(OH)_2$ at 364, 588, and 950 nm are due to the $^3A_2 \rightarrow {}^3T_1(^3P)$, $^3A_2 \rightarrow {}^3T_1(^3F)$, and $^3A_2 \rightarrow {}^3T_2(^3F)$ transitions, respectively. These transitions are attributed on the
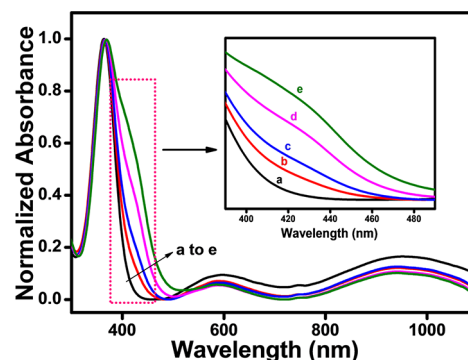

Figure 1. Normalized absorption spectra of (a) pristine α-$Ni_1(OH)_2$ sheets, (b) α-$Ni_1(OH)_2$-$Ag_{0.5}$, (c) α-$Ni_1(OH)_2$-Ag_1, (d) α-$Ni_1(OH)_2$-Ag_2, and (e) α-$Ni_1(OH)_2$-Ag_3 CMs (inset: enlarged view of UV−vis absorption spectra of α-$Ni_1(OH)_2$-$Ag_{0.5−3}$ CMs).

basis of the d^8 system of Ni^{2+} in octahedral symmetry.[12] As expected, an additional characteristic absorbance band was noticed for α-$Ni_1(OH)_2$-$Ag_{0.5-3}$ CMs to the deposition of AgNPs. Upon the deposition of different concentrations of AgNPs on the pristine α-$Ni_1(OH)_2$ sheet, a new SPR band was observed at 423, 427, 429, and 431 nm with gradual increases of $Ag_{0.5}NPs$, Ag_1NPs, Ag_2NPs, and Ag_3NPs on the α-$Ni_1(OH)_2$ sheet (Figure 1b–e and inset), respectively, and the presence of AgNPs did not change the absorption spectra of α-$Ni_1(OH)_2$ sheets at 364, 588, and 950 nm. The gradual redshift observed in the absorption spectra of the AgNPs indicates the formation of different sizes of AgNPs in the α-$Ni_1(OH)_2$-Ag CMs.[29]

Figure 2A–E shows the TEM images of pristine α-$Ni_1(OH)_2$ sheets and $Ag_{0.5-3}NPs$ deposited on α-$Ni_1(OH)_2$ sheets. In α-$Ni_1(OH)_2$-$Ag_{0.5}$ CMs, a few number with smaller sizes of AgNPs are deposited on the α-$Ni_1(OH)_2$ sheets (Figure 2B). When the concentration of AgNPs increased from $Ag_{0.5}$ to Ag_1 (Figure 2C), Ag_2 (Figure 2D), and Ag_3 (Figure 2E), the number and size of the AgNPs deposited on the α-$Ni_1(OH)_2$ sheets increased gradually with uniform deposition of AgNPs ($Ag_{0.5-3}$) on the α-$Ni_1(OH)_2$ sheets. The average size of AgNPs for the α-$Ni_1(OH)_2$-$Ag_{0.5}$, α-$Ni_1(OH)_2$-Ag_1, α-$Ni_1(OH)_2$-Ag_2, and α-$Ni_1(OH)_2$-Ag_3 CMs were found to be 3.2, 4.4, 7.2, and 8.8 nm, respectively, and their corresponding histograms of particle size distribution are shown in Figure S1A–D. Figure 2 and Figure S1 show that the size of the AgNPs increased upon increasing the Ag concentration and that at higher Ag concentration, the AgNPs are closed deposited on α-$Ni_1(OH)_2$ sheets. The formation of AgNPs on the α-$Ni_1(OH)_2$ sheets (α-$Ni_1(OH)_2$-Ag_2 CMs) was further confirmed by recording the HAADF-STEM-EDS mapping images (Figure 3A–E). The presence and arrangement of nickel (yellow), silver (red), and oxygen (pink) are shown in Figure 3C–E, respectively, and the overlay of these atoms are shown in Figure 3B. These HAADF-TEM-EDS mapping images clearly shows the presence of AgNPs on the α-$Ni_1(OH)_2$ sheets. In addition, the SEM-EDS mapping images were also recorded for α-$Ni_1(OH)_2$-Ag_2 CMs to further confirm the deposition of AgNPs on the α-$Ni_1(OH)_2$ sheets (Figure S2A–E). The presence and arrangement of Ni (red), Ag (blue), and O (green) elements are shown in Figure S2B–D, respectively, and the corresponding overlay of these elements are shown in Figure S2E.

The XRD patterns of the α-$Ni_1(OH)_2$-$Ag_{0.5-3}$ CMs samples recorded immediately after preparation (Figure 4) show that AgNPs with different concentrations are deposited on the α-$Ni_1(OH)_2$ sheets. The diffraction peaks observed at 12.3 and 23.6° was ascribed to the {003} and {006} planes of the α-$Ni_1(OH)_2$ sheets, respectively (JCPDS 38-0715). Further, the new characteristic diffraction peak observed at 38.6° corresponds to the {111} plane of Ag for AgNPs (JCPDS 04-0784) on α-$Ni_1(OH)_2$ sheets, and the other diffraction peaks observed in Figure 4 was assigned to the SiO_2 glass plate (JCPDS 89-7499). Upon increasing the concentration of Ag from $Ag_{0.5}$ to Ag_3 on the α-$Ni_1(OH)_2$ sheets (Figure 4B–E), the intensity of diffraction peaks corresponding to the AgNPs increased, whereas the intensity of α-$Ni_1(OH)_2$ was not changed. The XRD patterns of all the samples were recorded after 1 month of preparation (Figure S3) and compared with the XRD patterns recorded immediately after preparation. The diffraction patterns recorded after 1 month matched well with the earlier recorded XRD patterns of the α-Ni(OH)$_2$-AgNP
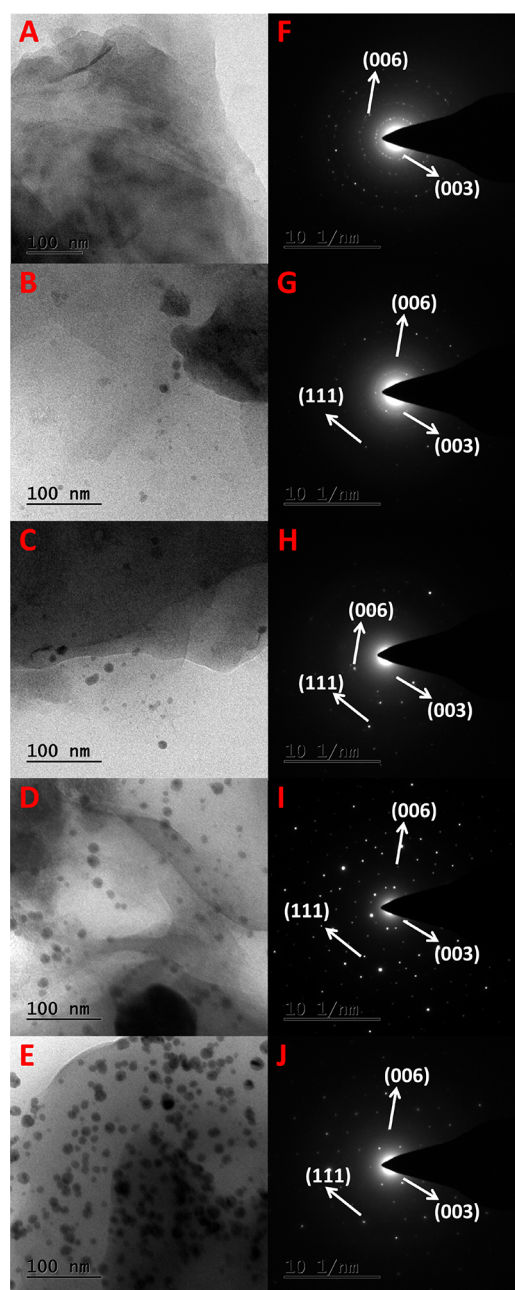

Figure 2. TEM images of (A) pristine α-$Ni_1(OH)_2$ sheets, (B) α-$Ni_1(OH)_2$-$Ag_{0.5}$, (C) α-$Ni_1(OH)_2$-Ag_1, (D) α-$Ni_1(OH)_2$-Ag_2, and (E) α-$Ni_1(OH)_2$-Ag_3 CMs and (F–J) their corresponding SAED patterns.

samples. This observation shows that the samples were stable for more than a month. Figure 5A shows the XPS survey spectrum recorded for α-$Ni_1(OH)_2$-Ag_2 CMs confirming the presence of Ni, O, and Ag. The high-resolution XPS spectrum (Figure 5B) shows the binding energy peaks at 855.4 and 872.8 eV corresponding to Ni $2p_{3/2}$ and Ni $2p_{1/2}$, respectively, which are characteristic to α-Ni(OH)$_2$ and in good arrangement with the reported XPS.[30] Figure 5C shows the high-resolution spectrum with peaks at 367.4 and 373.6 eV corresponding to Ag $3d_{5/2}$ and Ag $3d_{3/2}$, respectively.[31] In addition, the O 1s peak was observed at 531.5 eV (Figure 5D) for the α-$Ni_1(OH)_2$-Ag_2 CMs. ATR-FTIR spectra were recorded to further confirm the existence of Ni(OH)$_2$/TPDT silane (Figure S4). The IR absorption band observed
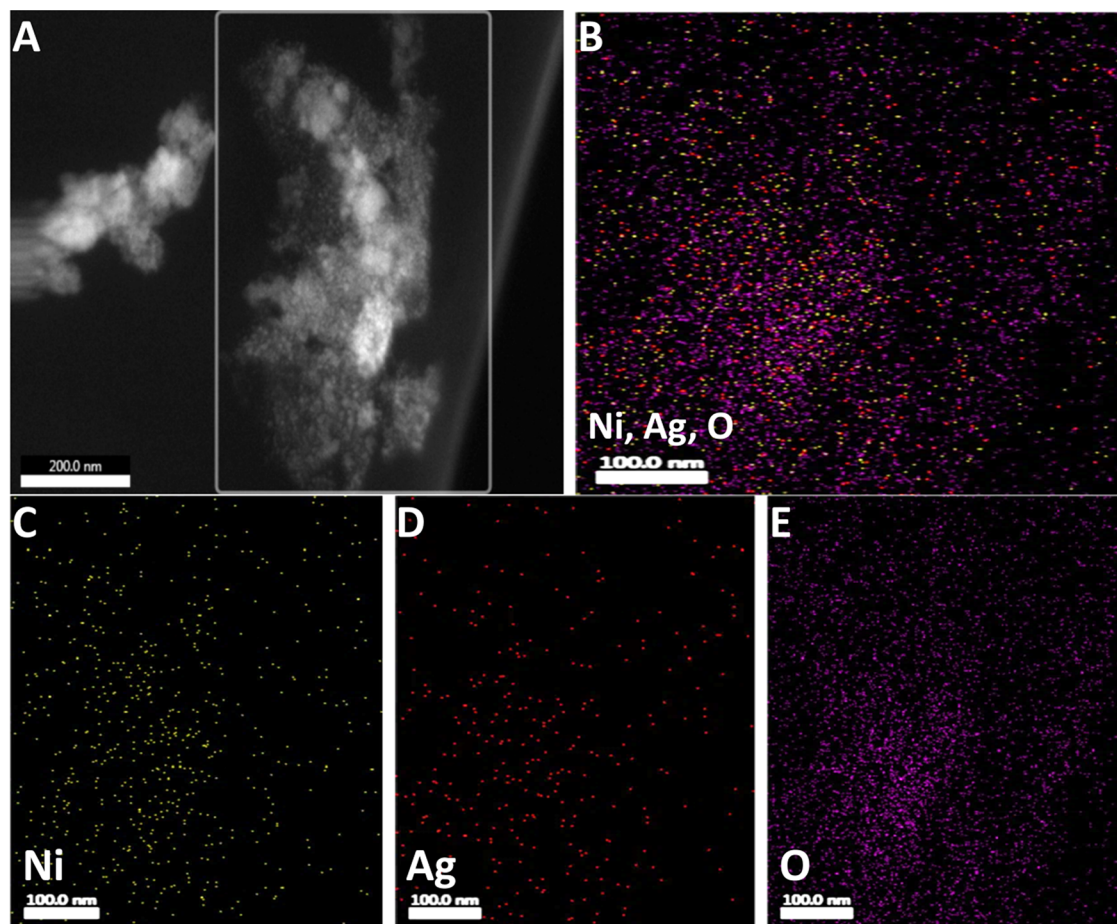
Figure 3. (A−E) HAADF-STEM-EDS mapping images of α-Ni$_1$(OH)$_2$-Ag$_2$ CMs [(B) Ni, Ag, and O; (C) Ni, yellow; (D) Ag, red; and (E) O, pink].
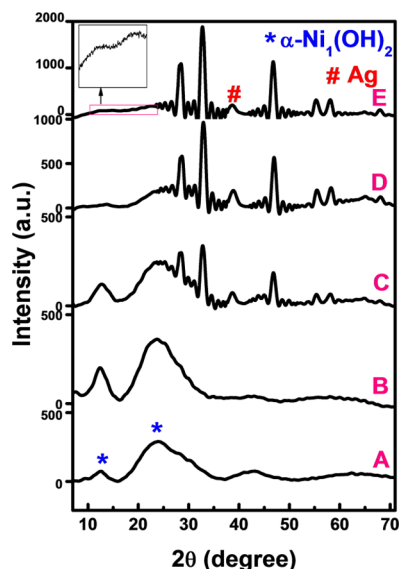
Figure 4. XRD patterns of the (A) pristine α-Ni$_1$(OH)$_2$ sheets, (B) α-Ni$_1$(OH)$_2$-Ag$_{0.5}$, (C) α-Ni$_1$(OH)$_2$-Ag$_1$, (D) α-Ni$_1$(OH)$_2$-Ag$_2$, and (E) α-Ni$_1$(OH)$_2$-Ag$_3$ CMs.

at 463 cm^{-1} corresponds to the Ni−OH stretching mode,[6] and the other band observed at 1064 cm^{-1} corresponds to the stretching vibration of Si−O−Si bond in TPDT silane.[32]

3.2. Optical Sensing of Hg^{2+} Ions. The absorption spectral changes observed for the α-Ni$_1$(OH)$_2$-Ag$_{0.5}$ (Figure 6A), α-Ni$_1$(OH)$_2$-Ag$_1$ (Figure 6B), α-Ni$_1$(OH)$_2$-Ag$_2$ (Figure 6C), and α-Ni$_1$(OH)$_2$-Ag$_3$CMs (Figure 6D) upon the addition of 25 μM Hg^{2+} ions to the corresponding solution are shown in Figure 6. The spectral changes observed upon the addition of 25 μM Hg^{2+} ions to other control samples, such as α-Ni$_1$(OH)$_2$/TPDT (Figure 6E) and AgNPs/TPDT (Figure 6F), and their corresponding intensity difference bar diagrams are shown in Figure 6G. The addition of 25 μM Hg^{2+} ions to α-Ni$_1$(OH)$_2$/TPDT did not bring about any change in the absorbance intensity (Figure 6E). Meanwhile, the absorbance intensity of the AgNPs was significantly decreased for α-Ni$_1$(OH)$_2$-Ag$_{0.5-3}$ CMs (Figure 6A−D), which indicates the redox interaction between the Ag in the α-Ni$_1$(OH)$_2$-Ag$_{0.5-3}$ CMs and Hg^{2+} ions that caused a change in the absorbance of the AgNPs.[33] This decrease in AgNP absorbance intensity was more pronounced when the concentration of Ag was increased from Ag$_{0.5}$ to Ag$_2$ and decreased when increasing the Ag concentration to Ag$_3$ (Figure 6G).This can be attributed to the number and size of AgNPs on the α-Ni$_1$(OH)$_2$ sheets. In the α-Ni$_1$(OH)$_2$-Ag$_2$ CMs, the number and size of AgNPs with uniform deposition shows the best optical sensing of Hg^{2+}ions (Figure 2D). The change in absorption intensity for pristine AgNPs/TPDT upon the addition of 25 μM Hg^{2+} ions (Figure 6F) is lower when compared to α-Ni$_1$(OH)$_2$-Ag$_{0.5-3}$ CMs (Figure 6A−D). From the absorption spectral changes of pristine α-Ni$_1$(OH)$_2$/TPDT, α-Ni$_1$(OH)$_2$-Ag$_{0.5-3}$ CMs, and
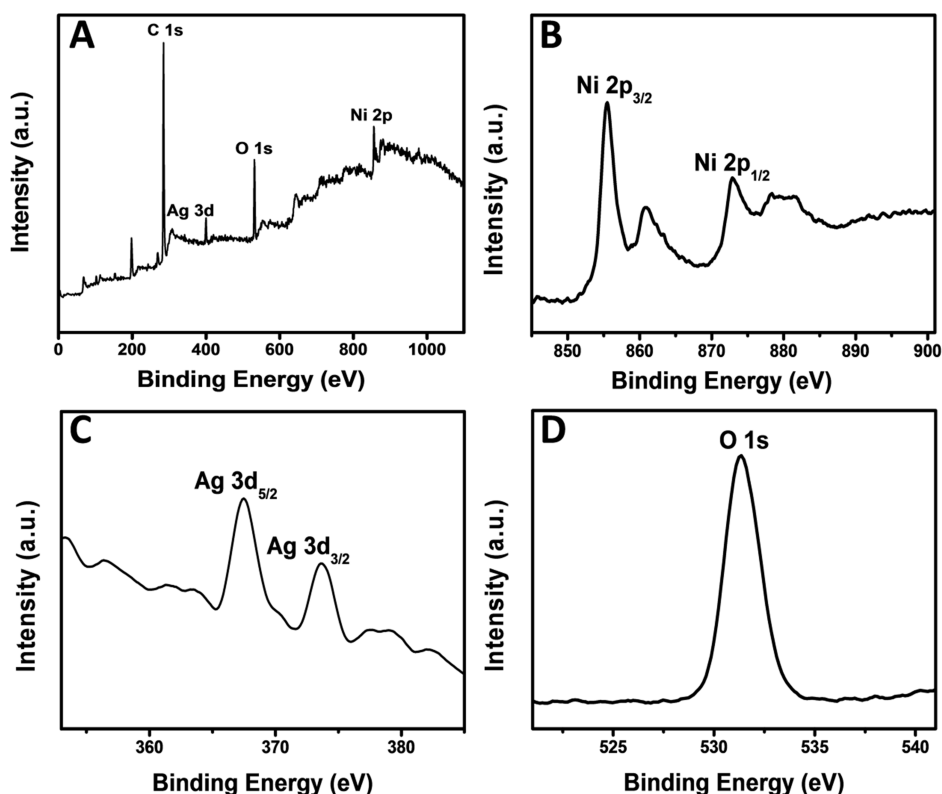
Figure 5. (A) XPS survey spectrum of α-$Ni_1(OH)_2$-Ag_2 CMs and high-resolution XPS spectra of (B) Ni 2p, (C) Ag 3d, and (D) O 1s.

pristine AgNPs/TPDT, it is concluded that the combination of both α-$Ni(OH)_2$ and AgNPs with an optimum concentration of AgNPs on α-$Ni(OH)_2$ shows best optical sensing property of Hg^{2+} ions. The effective sensing of Hg^{2+} ions may be attributed to the charge transfer interaction between α-$Ni(OH)_2$ and AgNPs in the α-$Ni(OH)_2$-AgNPs and the synergistic effect of the AgNPs and α-$Ni(OH)_2$ sheets.[34−36]

Figure 7A shows the enlarged view of the absorption spectral intensity changes recorded for the α-$Ni(OH)_2$-Ag_2CMs upon each addition of 5 μM Hg^{2+} ions, and the inset figure shows the complete spectra of the same. The absorption intensity of AgNPs was linearly decreased while increasing the concentration of Hg^{2+} ions due to the redox interaction between the Ag in the α-$Ni(OH)_2$-Ag_2 CMs and Hg^{2+} ions.[33,37]Figure 7B shows the corresponding plot of difference in AgNPs absorption intensity changes (I_d) at 422 nm against the concentration of Hg^{2+} ions (in the absence and presence of each addition of 5 μM Hg^{2+} ions) for α-$Ni_1(OH)_2$-Ag_2 CMs. Figure 7B shows a linear range from 5 to 50 μM for Hg^{2+} ions with an R^2 value of 0.9909 (a slope of 3.963×10^{-4}), and the limit of detection (LOD) was calculated to be 100.8 nM using the IUPAC-recommended formula.[38]Figure S5 shows the bar diagram and photograph image (Figure S5, inset) of the selective colorimetric sensing of Hg^{2+} ions (25 μM) in the presence of 100 μM different environmentally applicable metal ion interference like $MgCl_2$, Na_2SO_4, $CaCl_2$, $ZnCl_2$, $Ni(NO_3)_2$, $CuSO_4.5H_2O$, $CdCl_2$, $CoCl_2.6H_2O$, KNO_3, $PbCl_2$, $FeCl_2$, KCl, KBr, and NaCl ions to α -$Ni_1(OH)_2$-Ag_2 CMs. The disappearance of color observed upon the Hg^{2+} ion addition to α-$Ni_1(OH)_2$-Ag_2 CMs showed the selective sensing of Hg^{2+} ions in the presence of interference metal ions of 100 μM. The colorimetric detection limit was found to be 25 μM Hg^{2+} ions.

3.3. AgHg Amalgam Formation. The formation of AgHg amalgam can be assigned to the difference in the electro-chemical potentials of the Ag^+/Ag couple (0.80 V vs SHE) and Hg^{2+}/Hg couple (0.85 V vs SHE).[37] Hence, the Hg^{2+} ions possess enough electrochemical potential to oxidize Ag^0 to Ag^+ ions. The decrease in the absorption intensity observed for AgNPs at 422 nm upon the addition of Hg^{2+} ions to α-$Ni_1(OH)_2$-Ag_2 CMs reveals that the Hg^{2+} ions interact with the deposited AgNPs on α-$Ni(OH)_2$ sheets with the formation of AgHg amalgam,[39] which leads to the size reduction of AgNPs (size reduced to ~3 nm) and some aggregation[40] (Figure 8A,B). During Hg^{2+} ions sensing, after each addition of Hg^{2+} ions to the α-$Ni_1(OH)_2$-Ag_2 CMs (Figure 7A), the absorbance intensity of Ag was considerably quenched due to the redox interaction of Hg^{2+} ions with Ag in the α-$Ni_1(OH)_2$-Ag_2 CMs with the formation of AgHg amalgam.[39] The absorption spectral changes (Figure 7A) and the TEM images (Figure 8A,B) observed for the α-$Ni_1(OH)_2$-Ag_2 CMs upon the addition of Hg^{2+} ions clearly supports the AgHg amalgam formation. The XRD pattern recorded for the α-$Ni_1(OH)_2$-Ag_2 CMs after the addition of 25 μM Hg^{2+} ions (Figure S6) showed the disappearance of the XRD peak due to Ag, which confirms the AgHg amalgam formation. The SEM-EDS mapping images were also recorded for α-$Ni_1(OH)_2$-Ag_2 CMs after the addition of 25 μM Hg^{2+} ions to further confirm the presence of Hg in the α-$Ni_1(OH)_2$-Ag_2 CMs (Figure S7). The presence and arrangement of Ni (red), Ag (green), O (blue), and Hg (cyan) elements are shown in Figure S7B−E, respectively, and the overlay of these elements are shown in Figure S7F.

3.4. Real Sample Analysis. To find out the practical applicability of the prepared α-$Ni_1(OH)_2$-Ag_2 CMs for the sensing of Hg^{2+} ions, three different water samples (borewell
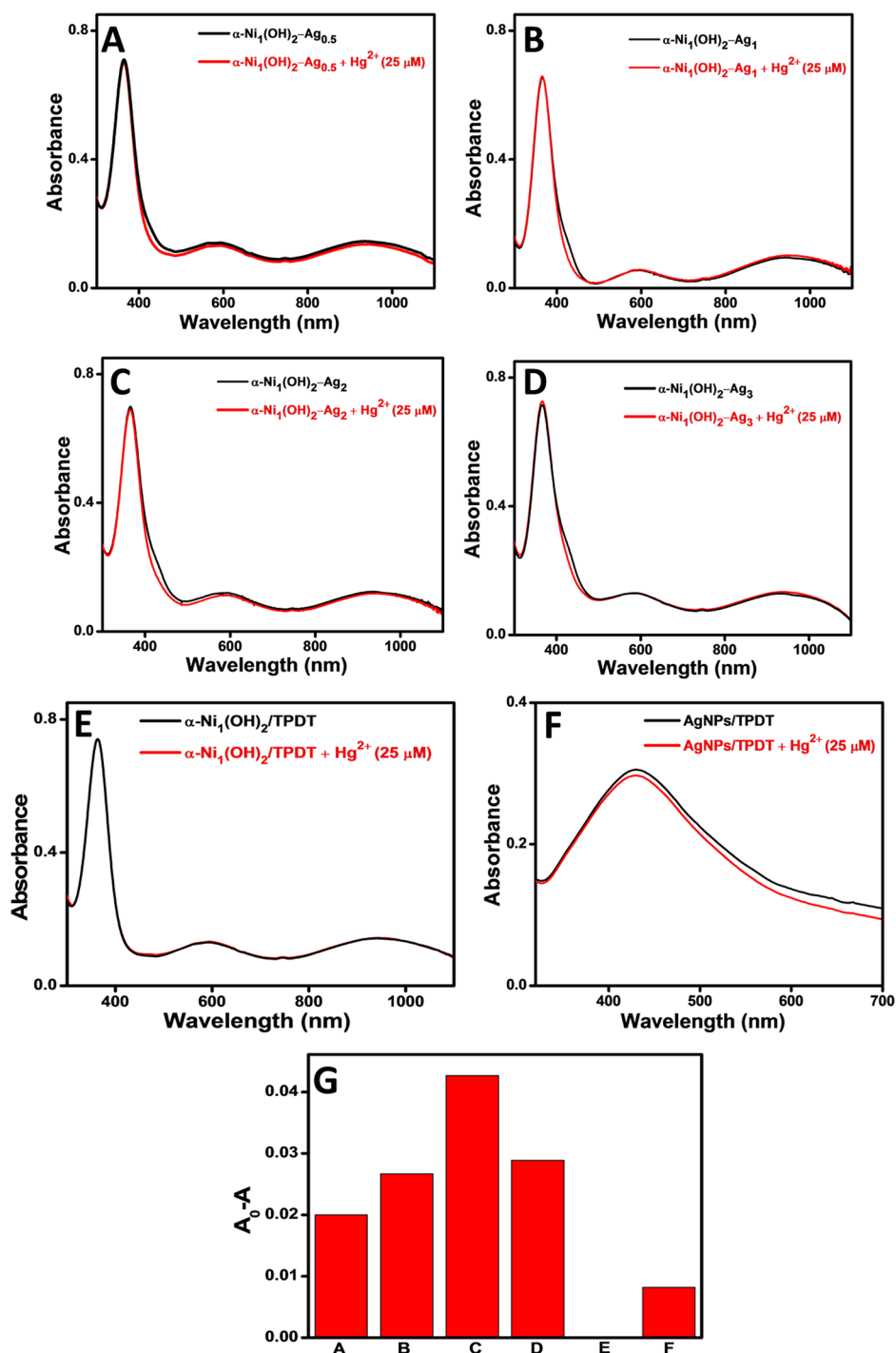
Figure 6. UV−vis absorption spectral changes recorded upon the addition of 25 μM Hg^{2+} ions to (A) α-$Ni_1(OH)_2$-$Ag_{0.5}$, (B) α-$Ni_1(OH)_2$-Ag_1, (C) α-$Ni_1(OH)_2$-Ag_2, (D) α-$Ni_1(OH)_2$-Ag_3 CMs, (E) pristine α-$Ni_1(OH)_2$/TPDT, (F) AgNPs/TPDT, and (G) the corresponding bar diagram.

water, pond water, and river water) were spiked with different concentrations of Hg^{2+} ions and analyzed. All the water samples were filtered using a filter paper before the experiment. From the observation, the recovery was calculated, and the results are summarized in Table S1. The results clearly suggests that the α-$Ni_1(OH)_2$-Ag_2 CMs can be used for the sensing of Hg^{2+} ions in real water samples.

4. CONCLUSIONS

In conclusion, the different concentrations of AgNPs ($Ag_{0.5}$, Ag_1, Ag_2, and Ag_3) deposited on pristine α-$Ni_1(OH)_2$ sheets

(α-$Ni_1(OH)_2$-$Ag_{0.5-3}$ CMs) were synthesized by a facile method at room temperature using N-[3(trimethoxysilyl)-propyl]diethylenetriamine silane without using an external reducing agent, and aminosilane acts as both reducing and stabilizing agent. The α-$Ni_1(OH)_2$-$Ag_{0.5-3}$ CMs were characterized using UV−vis absorption spectroscopy, TEM, XRD, XPS, and ATR-FTIR and confirmed the deposition of AgNPs on the α-$Ni_1(OH)_2$ sheets. The HAADF-STEM-EDS mapping images clearly revealed the deposition of AgNPs on the α-$Ni_1(OH)_2$ sheets. An optimum concentration of AgNPs on the α-$Ni_1(OH)_2$ sheets and the number and size of deposited
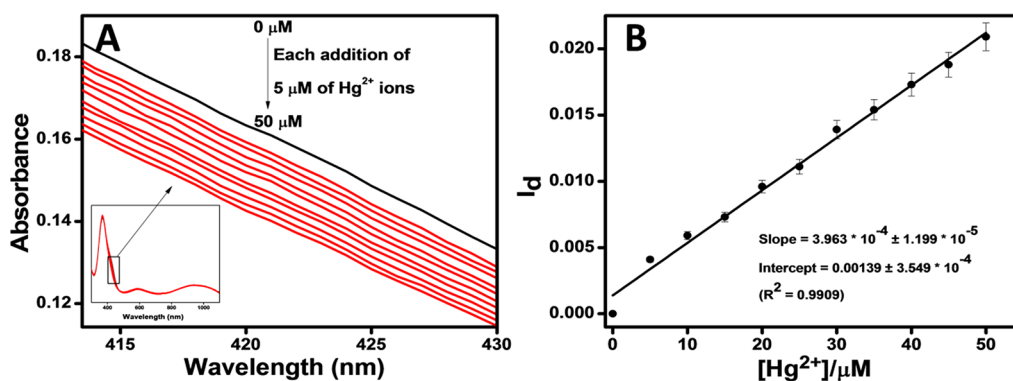
Figure 7. (A) Enlarged view of UV−vis absorption spectral changes recorded for α-Ni$_1$(OH)$_2$-Ag$_2$ CMs upon each addition of 5 μM Hg^{2+} ions (inset: UV−vis absorption spectra of α-Ni$_1$(OH)$_2$-Ag$_2$ CMs upon each addition of 5 μM Hg^{2+} ions) and (B) corresponding plot of the AgNP absorption intensity difference at 422 nm (I_d) in the absence and presence of each addition of 5 μM Hg^{2+} ions against concentration of the Hg^{2+} ions (R^2 = 0.991).
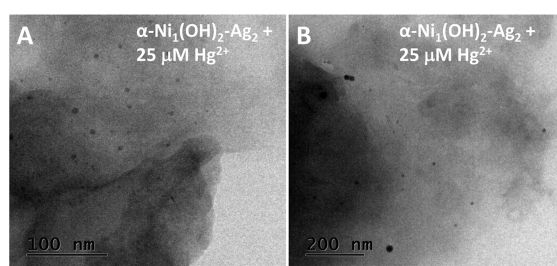
Figure 8. (A and B) TEM images recorded at different scale bars for α-Ni$_1$(OH)$_2$-Ag$_2$ CMs after the addition of 25 μM Hg^{2+} ions.

AgNPs are found to influence the sensing of α-Ni$_1$(OH)$_2$-Ag$_2$ CMs. The α-Ni$_1$(OH)$_2$-Ag$_2$ CMs showed the best optical and colorimetric sensing activity when compared to that of other CMs, pristine α-Ni$_1$(OH)$_2$ sheets, and AgNPs/TPDT. To the best our knowledge, this is the first report where the facile synthesis of deposition of AgNPs on a α-Ni$_1$(OH)$_2$ sheet using amine-functionalized silane is developed without using an external reducing agent and its application in optical and colorimetric sensing of Hg^{2+} ions is determined.

ASSOCIATED CONTENT

Supporting Information

The Supporting Information is available free of charge at https://pubs.acs.org/doi/10.1021/acsomega.2c05812.

Figure S1) Histogram; (Figure S2) SEM-EDS mapping images; (Figure S3) XRD patterns; (Figure S4) ATR-FTIR; (Figure S5) photograph image; (Figure S6) XRD pattern; (Figure S7) SEM-EDS mapping images; (Table S1) real sample analysis table (PDF)

AUTHOR INFORMATION

Corresponding Authors

Sivakumar Shanmugam − Department of Organic Chemistry, School of Chemistry, Madurai Kamaraj University, Madurai 625021, India; orcid.org/0000-0003-4087-7686; Email: shivazzen@mkuniversity.org

Ramasamy Ramaraj − School of Chemistry, Centre for Photoelectrochemistry, Madurai Kamaraj University, Madurai 625021, India; orcid.org/0000-0003-2242-5483; Email: ramarajr@yahoo.com

Authors

Manickam Sundarapandi − School of Chemistry, Centre for Photoelectrochemistry, Madurai Kamaraj University, Madurai 625021, India

Raju Praveen − School of Chemistry, Centre for Photoelectrochemistry, Madurai Kamaraj University, Madurai 625021, India

Complete contact information is available at:
https://pubs.acs.org/10.1021/acsomega.2c05812

Notes

The authors declare no competing financial interest.

ACKNOWLEDGMENTS

REFERENCES

(1) Hashimoto, Y.; Seniutinas, G.; Balčytis, A.; Juodkazis, S.; Nishijima, Y. Au-Ag-Cu Nano-Alloys: Tailoring of Permittivity. *Sci. Rep.* 2016, 6, 25010.

(2) Li, T. T.; He, C.; Zhang, W. X.; Cheng, M. Structural and Melting Properties of Cu-Ni Clusters: A Simulation Study. *J. Alloy. Compd.* 2018, 752, 76−84.

(3) Albrecht, G.; Ubl, M.; Kaiser, S.; Giessen, H.; Hentschel, M. Comprehensive Study of Plasmonic Materials in the Visible and Near-Infrared: Linear, Refractory, and Nonlinear Optical Properties. *ACS Photonics* 2018, 5, 1058−1067.

(4) Xu, Z.; He, X.; Liang, M.; Sun, L.; Li, D.; Xie, K.; Liao, L. Catalytic Reduction of 4-Nitrophenol over Graphene Supported Cu@Ni Bimetallic Nanowires. *Mater. Chem. Phys.* 2019, 227, 64−71.

(5) Gao, M.; Sheng, W.; Zhuang, Z.; Fang, Q.; Gu, S.; Jiang, J.; Yan, Y. Efficient Water Oxidation Using Nanostructured α-Nickel-Hydroxide as an Electrocatalyst. *J. Am. Chem. Soc.* 2014, 136, 7077−7084.

(6) Neiva, E. G. C.; Oliveira, M. M.; Bergamini, M. F.; Marcolino, L. H.; Zarbin, A. J. G. One Material, Multiple Functions: graphene/Ni(OH)$_2$ Thin Films Applied in Batteries, Electrochromism and Sensors. *Sci. Rep.* 2016, 6, 33806.

(7) Lynch, B. B.; Kelliher, A. P.; Anderson, B. D.; Japit, A.; Spencer, M. A.; Rizvi, M. H.; Sarac, M. F.; Augustyn, V.; Tracy, J. B. Sulfidation and Selenidation of Nickel Nanoparticles. *Carbon Energy* 2021, 3, 582.

(8) Xu, L.; Ding, Y.-S.; Chen, C.-H.; Zhao, L.; Rimkus, C.; Joesten, R.; Suib, S. L. 3D Flowerlike α-Nickel Hydroxide with Enhanced Electrochemical Activity Synthesized by Microwave-Assisted Hydrothermal Method. *Chem. Mater.* 2008, 20, 308−316.

(9) Dong, L.; Chu, Y.; Sun, W. Controllable Synthesis of Nickel Hydroxide and Porous Nickel Oxide Nanostructures with Different Morphologies. *Chem. − Eur. J.* 2008, 14, 5064−5072.

(10) Matsui, K.; Kyotani, T.; Tomita, A. Hydrothermal Synthesis of Single-Crystal Ni(OH)₂ Nanorods in a Carbon-Coated Anodic Alumina Film. *Adv. Mater.* 2002, 14, 1216−1219.

(11) Du, H.; Wang, Y.; Yuan, H.; Jiao, L. Facile Synthesis and High Capacitive Performance of 3D Hierarchical Ni(OH)₂ Microspheres. *Electrochim. Acta* 2016, 196, 84−91.

(12) Harvey, A.; He, X.; Godwin, I. J.; Backes, C.; McAteer, D.; Berner, N. C.; McEvoy, N.; Ferguson, A.; Shmeliov, A.; Lyons, M. E. G.; Nicolosi, V.; Duesberg, G. S.; Donegan, J. F.; Coleman, J. N. Production of Ni(OH)₂ Nanosheets by Liquid Phase Exfoliation: From Optical Properties to Electrochemical Applications. *J. Mater. Chem. A* 2016, 4, 11046−11059.

(13) Yan, J.; Kong, L.; Ji, Y.; White, J.; Li, Y.; Zhang, J.; An, P.; Liu, S.; Lee, S.-T.; Ma, T. Single Atom Tungsten Doped Ultrathin α-Ni(OH)₂ for Enhanced Electrocatalytic Water Oxidation. *Nat. Commun.* 2019, 10, 2149.

(14) Taniguchi, A.; Kubota, Y.; Matsushita, N.; Ishii, K.; Nguyen, T. K. N.; Uchikoshi, T.; Suzuki, Y. Sequenced Successive Ionic Layer Adsorption and Reaction for Rational Design of Ni(OH)₂/FeOOH Heterostructures with Tailored Catalytic Properties. *ACS Appl. Energy Mater.* 2021, 4, 8252−8261.

(15) Zhang, L.; Wang, G.; Jin, Z. Growth of Zn₀.₅Cd₀.₅S/α-Ni(OH)₂ Heterojunction by a Facile Hydrothermal Transformation Efficiently Boosting Photocatalytic Hydrogen Production. *New J. Chem.* 2019, 43, 6411−6421.

(16) Zhang, C.; Li, Z.; Jiang, S. Z.; Li, C. H.; Xu, S. C.; Yu, J.; Li, Z.; Wang, M. H.; Liu, A. H.; Man, B. Y. U-Bent Fiber Optic SPR Sensor Based on graphene/AgNPs. *Sens. Actuators, B* 2017, 251, 127−133.

(17) Li, W.; Teng, C.; Sun, Y.; Cai, L.; Xu, J.-L.; Sun, M.; Li, X.; Yang, X.; Xiang, L.; Xie, D.; Ren, T. Sprayed, Scalable, Wearable, and Portable NO₂ Sensor Array Using Fully Flexible AgNPs-All-Carbon Nanostructures. *ACS Appl. Mater. Interfaces* 2018, 10, 34485−34493.

(18) Yan, P.; Ding, Z.; Li, X.; Dong, Y.; Fu, T.; Wu, Y. Colorimetric Sensor Array Based on Wulff-Type Boronate Functionalized AgNPs at Various pH for Bacteria Identification. *Anal. Chem.* 2019, 91, 12134−12137.

(19) Srichan, C.; Ekpanyapong, M.; Horprathum, M.; Eiamchai, P.; Nuntawong, N.; Phokharatkul, D.; Danvirutai, P.; Bohez, E.; Wisitsoraat, A.; Tuantranont, A. Highly-Sensitive Surface-Enhanced Raman Spectroscopy (SERS)-Based Chemical Sensor Using 3D Graphene Foam Decorated with Silver Nanoparticles as SERS Substrate. *Sci. Rep.* 2016, 6, 23733.

(20) Mortazavi-Derazkola, S.; Ebrahimzadeh, M. A.; Amiri, O.; Goli, H. R.; Rafiei, A.; Kardan, M.; Salavati-Niasari, M. Facile Green Synthesis and Characterization of Crataegus Microphylla Extract-Capped Silver Nanoparticles (CME@Ag-NPs) and Its Potential Antibacterial and Anticancer Activities against AGS and MCF-7 Human Cancer Cells. *J. Alloy. Compd.* 2020, 820, No. 153186.

(21) Jeevika, A.; Shankaran, D. R. Functionalized Silver Nanoparticles Probe for Visual Colorimetric Sensing of Mercury. *Mater. Res. Bull.* 2016, 83, 48−55.

(22) Liu, J.; Vellaisamy, K.; Yang, G.; Leung, C.-H.; Ma, D.-L. Luminescent Turn-on Detection of Hg(II) via the Quenching of an iridium(III) Complex by Hg(II)-Mediated Silver Nanoparticles. *Sci. Rep.* 2017, 7, 3620.

(23) Guo, N.; Xu, G.; Zhang, Q.; Song, P.; Xia, L. AgNPs Functionalized with Dithizone for the Detection of Hg²⁺ Based on Surface-Enhanced Raman Scattering Spectroscopy. *Plasmonics* 2022, 17, 1419−1426.

(24) Chen, L.; Li, J.; Chen, L. Colorimetric Detection of Mercury Species Based on Functionalized Gold Nanoparticles. *ACS Appl. Mater. Interfaces* 2014, 6, 15897−15904.

(25) Chen, L.; Fu, X.; Lu, W.; Chen, L. Highly Sensitive and Selective Colorimetric Sensing of Hg²⁺ Based on the Morphology Transition of Silver Nanoprisms. *ACS Appl. Mater. Interfaces* 2013, 5, 284−290.

(26) Wang, G.; Chen, Z.; Wang, W.; Yan, B.; Chen, L. Chemical Redox-Regulated Mesoporous Silica-Coated Gold Nanorods for Colorimetric Probing of Hg²⁺ and S²⁻. *Analyst* 2011, 136, 174−178.

(27) Jayabal, S.; Sathiyamurthi, R.; Ramaraj, R. Selective Sensing of Hg²⁺ Ions by Optical and Colorimetric Methods Using Gold Nanorods Embedded in a Functionalized Silicate Sol−gel Matrix. *J. Mater. Chem. A* 2014, 2, 8918−8925.

(28) Bharathi, S.; Fishelson, N.; Lev, O. Direct Synthesis and Characterization of Gold and Other Noble Metal Nanodispersions in Sol−Gel-Derived Organically Modified Silicates. *Langmuir* 1999, 15, 1929−1937.

(29) Bastús, N. G.; Piella, J.; Puntes, V. Quantifying the Sensitivity of Multipolar (Dipolar, Quadrupolar, and Octapolar) Surface Plasmon Resonances in Silver Nanoparticles: The Effect of Size, Composition, and Surface Coating. *Langmuir* 2016, 32, 290−300.

(30) Yan, J.; Fan, Z.; Sun, W.; Ning, G.; Wei, T.; Zhang, Q.; Zhang, R.; Zhi, L.; Wei, F. Advanced Asymmetric Supercapacitors Based on Ni(OH)₂/Graphene and Porous Graphene Electrodes with High Energy Density. *Adv. Funct. Mater.* 2012, 22, 2632−2641.

(31) Sharma, R.; Dhillon, A.; Kumar, D. Mentha-Stabilized Silver Nanoparticles for High-Performance Colorimetric Detection of Al(III) in Aqueous Systems. *Sci. Rep.* 2018, 8, 5189.

(32) Sundarapandi, M.; Shanmugam, S.; Ramaraj, R. Tuning Cu₂O Shell on Gold Nanocube Core Employing Amine-Functionalized Silane for Electrocatalytic Nitrite Detection. *ACS Appl. Nano Mater.* 2022, 5, 1674−1682.

(33) Rameshkumar, P.; Manivannan, S.; Ramaraj, R. Silver Nanoparticles Deposited on Amine-Functionalized Silica Spheres and Their Amalgamation-Based Spectral and Colorimetric Detection of Hg(II) Ions. *J. Nanopart. Res.* 2013, 15, 1639.

(34) Bao, F.; Tan, F.; Wang, W.; Qiao, X.; Chen, J. Facile Preparation of Ag/Ni(OH)₂ Composites with Enhanced Catalytic Activity for Reduction of 4-Nitrophenol. *RSC Adv.* 2017, 7, 14283−14289.

(35) Sheng, Q.; Liu, D.; Zheng, J. A Nonenzymatic Electrochemical Nitrite Sensor Based on Pt Nanoparticles Loaded Ni(OH)₂/multi-Walled Carbon Nanotubes Nanocomposites. *J. Electroanal. Chem.* 2017, 796, 9−16.

(36) Cai, R.; Jin, H.; Yang, D.; Lin, K.-T.; Chan, K.; Sun, J.; Chen, Z.; Zhang, X.; Tan, W. Generalized Preparation of Au NP @ Ni(OH)₂ Yolk-Shell NPs and Their Enhanced Catalytic Activity. *Nano Energy* 2020, 71, No. 104542.

(37) Harika, V. K.; Kumar, V. B.; Gedanken, A. One-Pot Sonochemical Synthesis of Hg−Ag Alloy Microspheres from Liquid Mercury. *Ultrason. Sonochem.* 2018, 40, 157−165.

(38) Committee, A. M. Recommendations for the Definition, Estimation and Use of the Detection Limit. *Analyst* 1987, 112, 199−204.

(39) Zangeneh Kamali, K.; Pandikumar, A.; Jayabal, S.; Ramaraj, R.; Lim, H. N.; Ong, B. H.; Bien, C. S. D.; Kee, Y. Y.; Huang, N. M. Amalgamation Based Optical and Colorimetric Sensing of mercury-(II) Ions with Silver@graphene Oxide Nanocomposite Materials. *Microchim. Acta* 2016, 183, 369−377.

(40) Deng, L.; Ouyang, X.; Jin, J.; Ma, C.; Jiang, Y.; Zheng, J.; Li, J.; Li, Y.; Tan, W.; Yang, R. Exploiting the Higher Specificity of Silver Amalgamation: Selective Detection of Mercury(II) by Forming Ag/Hg Amalgam. *Anal. Chem.* 2013, 85, 8594−8600.